molecules

MDPI

Article

Evidence of Cooperative Effects for the $Fe(phen)_2(NCS)_2$ Spin Crossover Molecular Complex in Polyaniline Plus Iron Magnetite

Wai Kiat Chin [1,†], Binny Tamang [2,†], M. Zaid Zaz [1], Arjun Subedi [1], Gauthami Viswan [1], Alpha T. N'Diaye [3], Rebecca Y. Lai [2,*] and Peter A. Dowben [1,*]

[1] Department of Physics and Astronomy, University of Nebraska-Lincoln, Lincoln, NE 68588, USA; wchin6@huskers.unl.edu (W.K.C.); zzaz2@huskers.unl.edu (M.Z.Z.); arjun.subedi@huskers.unl.edu (A.S.); gviswan2@huskers.unl.edu (G.V.)
[2] Department of Chemistry, University of Nebraska-Lincoln, Lincoln, NE 68588, USA; btamang2@huskers.unl.edu
[3] Advanced Light Source, Lawrence Berkeley National Laboratory, Berkeley, CA 94720, USA; atndiaye@lbl.gov
* Correspondence: rlai2@unl.edu (R.Y.L.); pdowben1@unl.edu (P.A.D.)
† These authors contributed equally to this work.

Abstract: The spin crossover complex $Fe(phen)_2(NCS)_2$ and its composite, $Fe(phen)_2(NCS)_2$, combined with the conducting polymer polyaniline (PANI) plus varying concentrations of iron magnetite (Fe_3O_4) nanoparticles were studied. A cooperative effect is evident from the hysteresis width in the plot of magnetic susceptibility multiplied by temperature versus temperature (χ_mT versus T) for $Fe(phen)_2(NCS)_2$ with PANI plus varying concentrations of Fe_3O_4 nanoparticles. The hysteresis width in the composites vary no more than 2 K with respect to the pristine $Fe(phen)_2(NCS)_2$ spin crossover crystallites despite the fact that there exists a high degree of miscibility of the $Fe(phen)_2(NCS)_2$ spin crossover complex with the PANI. The Fe_3O_4 nanoparticles in the $Fe(phen)_2(NCS)_2$ plus PANI composite tend to agglomerate at higher concentrations regardless of the spin state of $Fe(phen)_2(NCS)_2$. Of note is that the Fe_3O_4 nanoparticles are shown to be antiferromagnetically coupled with the $Fe(phen)_2(NCS)_2$ when $Fe(phen)_2(NCS)_2$ is in the high spin state.

Keywords: spin crossover composites; cooperative effects; molecular-based memory device; functional materials

Citation: Chin, W.K.; Tamang, B.; Zaz, M.Z.; Subedi, A.; Viswan, G.; N'Diaye, A.T.; Lai, R.Y.; Dowben, P.A. Evidence of Cooperative Effects for the $Fe(phen)_2(NCS)_2$ Spin Crossover Molecular Complex in Polyaniline Plus Iron Magnetite. *Molecules* **2024**, *29*, 4574. https://doi.org/10.3390/molecules29194574

Academic Editors: Igor Djerdj and Federico Totti

Received: 16 August 2024
Revised: 16 September 2024
Accepted: 19 September 2024
Published: 26 September 2024

1. Introduction

The study of the effects of mixing a conducting polymer with bi-stable spin crossover (SCO) molecular complexes is fairly recent and sparse [1–9]. Efforts have been made in an attempt to lower the on-state resistance of spin crossover molecular films by forming composites with various conducting polymers [1,3,4,6], largely with the goal of improving the utility of SCO film-based devices [4,10–20]. A previous study of a polymeric spin crossover $[Fe(Htrz)_2(trz)](BF)_4$ plus the conducting polymer polyaniline (PANI) showed a reduction in the hysteresis width in the χ_mT versus T, which is an indication of a reduced cooperative effect [5]. However, the cooperative effect of $[Fe(Htrz)_2(trz)](BF)_4$ was restored and enhanced following the addition of iron magnetite (Fe_3O_4) nanoparticles into the $[Fe(Htrz)_2(trz)](BF)_4$ plus PANI composite. This was understood to be due to the phase separation of $[Fe(Htrz)_2(trz)](BF)_4$ in the PANI matrix caused by the addition of Fe_3O_4 nanoparticles. Such a phase separation turned the miscible $[Fe(Htrz)_2(trz)](BF)_4$ plus PANI composite into immiscible domains of $[Fe(Htrz)_2(trz)](BF)_4$ and PANI, where the Fe_3O_4 nanoparticles are preferentially segregated to the $[Fe(Htrz)_2(trz)](BF)_4$ domains. Overall, the prior study has suggested that the miscibility gap in the SCO-polymer system could be easily perturbed.

Similarly, the spin crossover complex $Fe(phen)_2(NCS)_2$ has been much studied [21–41], and the spin state transition temperature for this complex is in the vicinity of 176 K [27–34,37–39]. Prior studies of Mn-doped and Zn-doped $Fe(phen)_2(NCS)_2$ thin films [38–40], as well as $[Fe(phen)_2(NCS)_2]$ crystallites coated with an organic, like glycerol [41], showed that the hysteresis width, in $\chi_m T$ versus T, varied depending on the dopant [38,39] and the coating layer [41], respectively. In this study, we observed that for $Fe(phen)_2(NCS)_2$ plus PANI plus varying concentrations of Fe_3O_4 nanoparticle composites, the hysteresis width of $\chi_m T$ versus T remains largely unchanged. The hysteresis width behavior of $Fe(phen)_2(NCS)_2$ plus PANI plus varying concentrations of Fe_3O_4 nanoparticles is starkly different from that of the $[Fe(Htrz)_2(trz)](BF)_4$ plus PANI plus Fe_3O_4 nanoparticles (1% loading by weight) [5], indicating that the dispersion of a spin crossover complex in PANI and the exchange between the spin crossover complex and the Fe_3O_4 nanoparticles, which is mediated by PANI, depends very much on the choice of spin crossover molecule. With this work, there are now examples of both ferromagnetic [5] and antiferromagnetic coupling between a spin crossover molecular complex and iron magnetite nanoparticles, mediated by polyaniline.

2. Experimental Details

All the reagents and solvents were used as received. Ammonium iron (II) sulfate hexahydrate (99%), aniline (99.8%), ammonium persulfate (APS), and hydrochloric acid (HCl) (ACS reagent, 37%) were purchased from Fisher Scientific (Hampton, NH, USA). 1–10 phenanthroline monohydrate was purchased from Chem-Impex (Wood Dale, IL, USA). Sodium thiocyanate (NaSCN) (99%) was purchased from Avantor (Radnor Township, PA, USA). Ethanol and methanol ($\geq$99.9%) were purchased from Aldrich (St. Louis, MO, USA). Iron (II, III) nano-powders (50–100 nm particle size, 97% trace metals) were purchased from Millipore Sigma (Burlington, MA, USA). The solutions used in this study were made with deionized (DI) water purified through a Millipore Synergy system (18.2 MΩ·cm, Millipore, Billerica, MA, USA).

The method used for the synthesis of $Fe(phen)_2(NCS)_2$ was adapted from the one used by Akabori et al. [42]. In brief, 1.95 g of ammonium iron (II) sulfate hexahydrate and 3.00 g of 1–10 phenanthroline were dissolved together in 200 mL of DI water, resulting in a dark-red solution. Next, 21 g of NaSCN was added to 15 mL of DI water to create a saturated solution, and this solution was added to the dark-red solution while stirring. Fine crystals were observed immediately, but the solution mixture was stirred for another four hours at room temperature to complete the reaction. The crude product was collected on Whatman filter paper and rinsed with methanol. It was further purified via recrystallization in methanol and dried in air. The purity was determined by IR spectroscopy (Supplementary Materials Figure S1).

The synthesis of PANI was adapted from the methods used by Tang et al. [43] and Adams et al. [44]. A solution containing 0.25 M aniline (683 µL) in 30 mL of DI water was placed in an ice bath with magnetic stirring at 800 rpm, and 0.25 M APS in 10 mL of 1 M HCl was added to the aniline solution. The solution was allowed to stir for six hours at 0 °C. A dark green precipitate began to form within the first half hour. After six hours, the reaction was left to proceed overnight with stirring at room temperature. The dark green precipitate was collected using ultracentrifugation at 4500 rpm for 30 min and washed several times with 1 M HCl, ethanol, and DI water.

The fabrication of the composite thin films of $Fe(phen)_2(NCS)_2$ plus PANI and $Fe(phen)_2(NCS)_2$ together with PANI and Fe_3O_4 nanoparticles was accomplished through a solvent approach. In total, 20 mg of $Fe(phen)_2(NCS)_2$ and 20 mg of PANI were added to 5 mL of methanol, and this mixture was sonicated in a Branson 2510R-MT bath sonicator at room temperature for 10 min to create a uniform dispersion. This mixture, also known as the 1:1 $Fe(phen)_2(NCS)_2$/PANI bi-composite, was then dried to completion in air prior to vibrating sample magnetometry (VSM) analysis. The 1:1 $Fe(phen)_2(NCS)_2$/PANI bi-composite ratio is emphasized in this work to make the comparison with the prior study of

the $[Fe(Htrz)_2(trz)](BF)_4$ plus PANI composite [5] more facile. To fabricate the tri-composite samples containing $Fe(phen)_2(NCS)_2$, PANI, and Fe_3O_4, different amounts (1, 5, and 10% by weight) of Fe_3O_4 nanoparticles were added to the 1:1 $Fe(phen)_2(NCS)_2$/PANI bi-composite and sonicated again for 10 min until uniformly dispersed. These samples were dried in air prior to VSM analysis.

The measurements of DC magnetic susceptibility times temperature ($\chi_m T$) were carried out in DynaCool PPMS from Quantum Design. The elemental mapping of iron and sulfur in the $[Fe(phen)_2(NCS)_2]$ and its composites was performed using the FEI Tecnai Osiris S/TEM with the means of energy-dispersive X-ray spectroscopy (EDAX) and high-angle annular dark-field imaging mode with a 200 kV accelerating voltage of scanning transmission electron microscopy (HAADF-STEM). The $Fe(phen)_2(NCS)_2$ and its composites plus polyaniline (PANI) plus various concentrations of Fe_3O_4 nanoparticle solutions were drop-casted on formvar/carbon 200 mesh copper TEM grids from Ted Pella.

The room temperature DC current-voltage I(V) measurements of $Fe(phen)_2(NCS)_2$ plus PANI plus Fe_3O_4 (10% loading by weight) drop-cast between two copper electrodes were taken using the two-point probe method and recorded using a 4200A SCS parameter analyzer connected to a Lakeshore cryogenic probe station. The measurements were carried out in the absence of visible light illumination and a sweep rate of 260 ms per data point.

The coupling between the $Fe(phen)_2(NCS)_2$ and Fe_3O_4 nanoparticles in the composite was probed with X-ray absorption spectroscopy (XAS) and X-ray magnetic circular dichroism spectroscopy (XMCD), as a function of temperature, at the Advanced Light Source (Lawrence Berkeley National Laboratory) beamline 6.3.1, with a constant circularly polarized light whose estimated degree of polarization was 0.66. Throughout the experiments, the XAS spectra were taken in the total electron yield mode across the Fe $L_{3,2}$ edges ranging from 700 eV to 735 eV with an alternating magnetic field of $\pm$1.5 T, which are anti-parallel ($\sigma^{\downarrow}$) and parallel ($\sigma^{\uparrow}$) with respect to the helicity of the incoming photon. The XMCD signal was later evaluated as a difference of the two XAS spectra taken with two oppositely applied magnetic fields.

3. Miscibility and Cooperativity

The intermolecular interactions, namely the cooperative effects [45–48], were examined through thermal hysteresis in terms of the magnetic susceptibility (χ_m) times temperature versus temperature, i.e., the hysteresis width in the plot of $\chi_m T$ versus T. The hysteresis width, in principle, is a measure of the strength of the cooperativity between adjacent SCO molecules, with a larger hysteresis width equivalent to stronger cooperative effects [45–48]. The hysteresis widths in the $\chi_m T$ versus T for $Fe(phen)_2(NCS)_2$ and for the combination of $Fe(phen)_2(NCS)_2$ plus PANI were 10.6 K and 11.3 K, respectively, as shown in Figure 1 (Supplementary Figure S4). The percentage error in the measured $\chi_m T$ versus T hysteresis width was less than 6%. The observed hysteresis width in this study is significantly larger than the 0.15 to 1.5 K [27,29,30,33,34] and 6.1–8.5 K [31] reported previously but roughly similar to the hysteresis width of Mn-doped and Zn-doped $Fe(phen)_2(NCS)_2$ thin films, which were 10 K [39] and 14 K [38]. This is surprising as this is very different from the example of $[Fe(Htrz)_2(trz)](BF)_4$, where a significant 7 K reduction of $\chi_m T$ versus T hysteresis width was observed upon mixing with PANI [5].

A comparison of the mixtures of $Fe(phen)_2(NCS)_2$ with PANI in the ratios of 1:2, 1:1, and 2:1, as seen in Figure 2, illustrates that the magnetization for the $Fe(phen)_2(NCS)_2$ to PANI in the ratio of 1:1 is slightly larger than that seen for the ratios of 1:2 and 2:1 $Fe(phen)_2(NCS)_2$ to PANI compositions. The temperature-dependent hysteresis varies only slightly, with the hysteresis loop ($\Delta T_{1/2}$) for both the 1:1 $Fe(phen)_2(NCS)_2$ to PANI and the 1:2 $Fe(phen)_2(NCS)_2$ to PANI bi-composite measuring ~11 K, but for the 2:1 $Fe(phen)_2(NCS)_2$ to PANI bi-composite, the hysteresis is ~12 K.

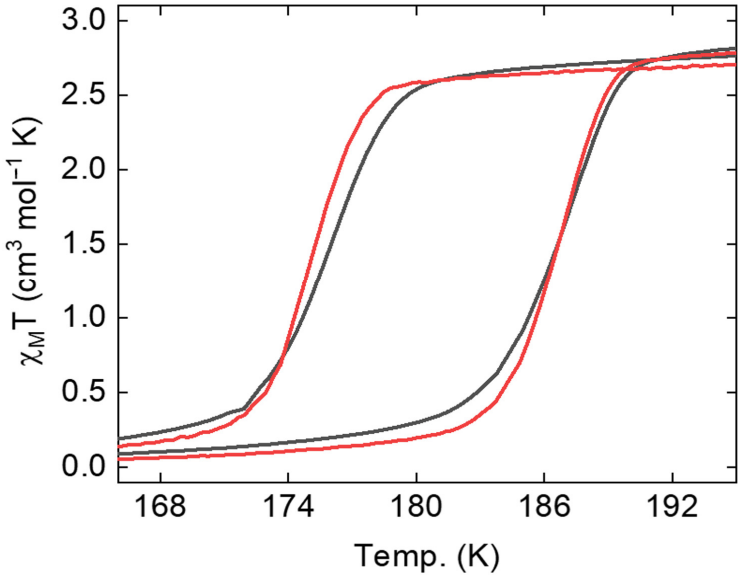

Figure 1. The enlarged view of the magnetic susceptibility time temperature, $\chi_M T$, versus T plot for $Fe(phen)_2(NCS)_2$ crystallites (gray) and its composite $Fe(phen)_2(NCS)_2$ plus PANI (1:1 $Fe(phen)_2(NCS)_2$/PANI weight %) plotted in red.

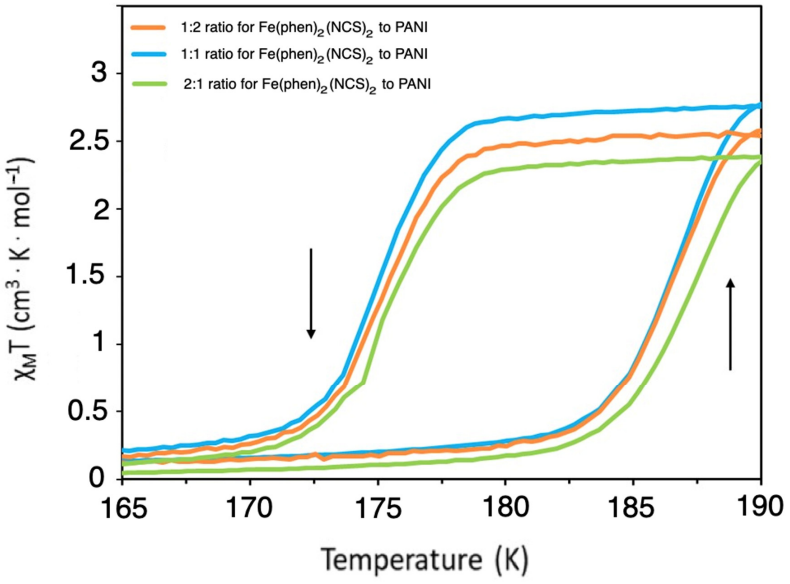

Figure 2. The thermal hysteresis behavior of $\chi_M T$ versus T for $Fe(phen)_2(NCS)_2$ to PANI bi-composites in the different ratios of 2:1 (green), 1:1 (blue), and 1:2 (orange). The arrows indicate increasing (up) and decreasing (down) temperature paths.

From the elemental mapping of both iron and sulfur of the $[Fe(phen)_2(NCS)_2]$ in the pristine $Fe(phen)_2(NCS)_2$ crystallites and the $Fe(phen)_2(NCS)_2$ plus PANI composite, respectively, in Figures 3 and 4, the fact that the $Fe(phen)_2(NCS)_2$ is uniformly distributed within the PANI matrix is clear. In other words, there is a high degree of miscibility of $Fe(phen)_2(NCS)_2$ within the PANI matrix. The two different spin crossover complexes, $[Fe(Htrz)_2(trz)](BF)_4$ and $Fe(phen)_2(NCS)_2$, while both are apparently miscible with the PANI, do not mix the same way in the PANI, judging from the differences in the changes to the hysteresis width in the $\chi_m T$ versus T seen with mixing $[Fe(Htrz)_2(trz)](BF)_4$ with PANI and not seen when $Fe(phen)_2(NCS)_2$ was mixed with PANI, as noted above. One notable difference between these two spin crossover molecules is that $[Fe(Htrz)_2(trz)](BF)_4$ is a polymeric spin crossover complex and $Fe(phen)_2(NCS)_2$ is not.

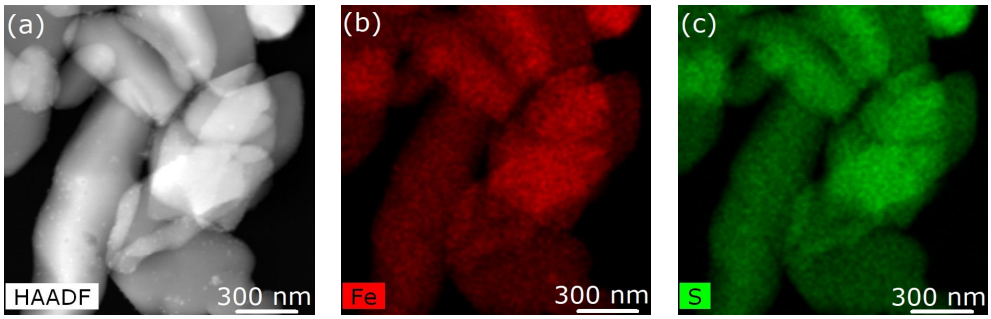

Figure 3. (**a**) Image of pristine $Fe(phen)_2(NCS)_2$ obtained using scanning transmission microscopy in high-angle annular dark-field mode. (**b**,**c**) Elemental mapping of iron and sulfur of the $[Fe(phen)_2(NCS)_2]$, respectively.

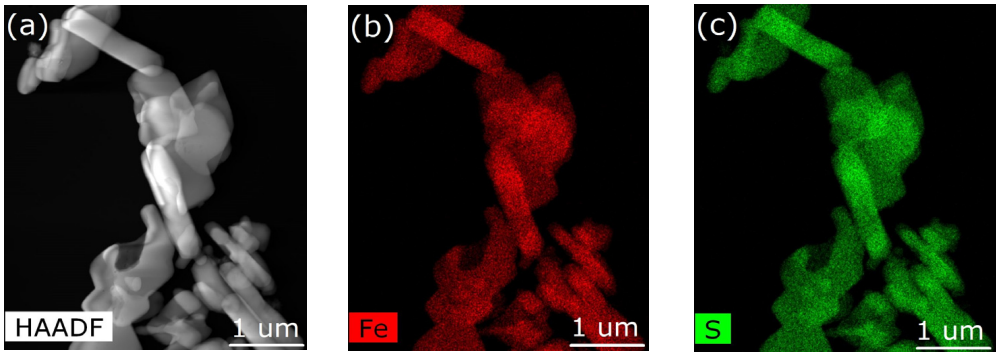

Figure 4. (**a**) Image of $Fe(phen)_2(NCS)_2$ combined with polyaniline (PANI) obtained using scanning transmission microscopy in high-angle annular dark-field mode. (**b**,**c**) Elemental mapping of iron and sulfur of the $[Fe(phen)_2(NCS)_2]$, respectively.

We offer two possible explanations as to why the cooperative effects (as indicated by the temperature-dependent hysteresis of the susceptibility) of $Fe(phen)_2(NCS)_2$ moieties mixed in the PANI remain largely unchanged. First, there could exist tiny $Fe(phen)_2(NCS)_2$ crystallites with the correct packing for enhancing the hysteresis [31] that are evenly distributed within the PANI matrix. For $Fe(phen)_2(NCS)_2$, the hysteresis width can also be affected by the crystallite quality [31,34]. Alternatively, there is the possibility of strong cooperativity between $Fe(phen)_2(NCS)_2$ moieties in widely distributed crystallites or PANI, which enhances the $\chi_m T$ versus T hysteresis observed in this study here. The large and unperturbed $\chi_m T$ versus T hysteresis suggests that PANI encapsulates the $Fe(phen)_2(NCS)_2$, which could enhance the overall cooperativity. Similar polymer-encapsulation-induced hysteresis enhancement of $[Fe(phen)_2(NCS)_2]$ has been reported [25,41]. The explanation is consistent with the observations where there is strong cooperativity for $Fe(phen)_2(NCS)_2$ when encapsulated by organics [7,9,25,41]. The latter explanation is consistent with the observed increased hysteretic spin transition behavior of $Fe(phen)_2(NCS)_2$ in several different embedding matrices [9].

4. Phase Separation and Cooperativity

With increasing Fe_3O_4 nanoparticle concentrations in the $Fe(phen)_2(NCS)_2$ plus PANI composite, the Fe_3O_4 nanoparticles tend to agglomerate and become less uniformly distributed (Figures 5b, 6b and 7b) in the PANI matrix, while the $Fe(phen)_2(NCS)_2$ remains uniformly distributed within the PANI, as indicated by the sulfur spatial map (Figures 5c, 6c and 7c). Although there is always a possibility that the coupling between the Fe_3O_4 nanoparticles could lead to magnetic frustration, this is excluded here as the overall paramagnetic susceptibility scales with the Fe_3O_4 nanoparticle concentration in the $Fe(phen)_2(NCS)_2$ plus PANI composite.

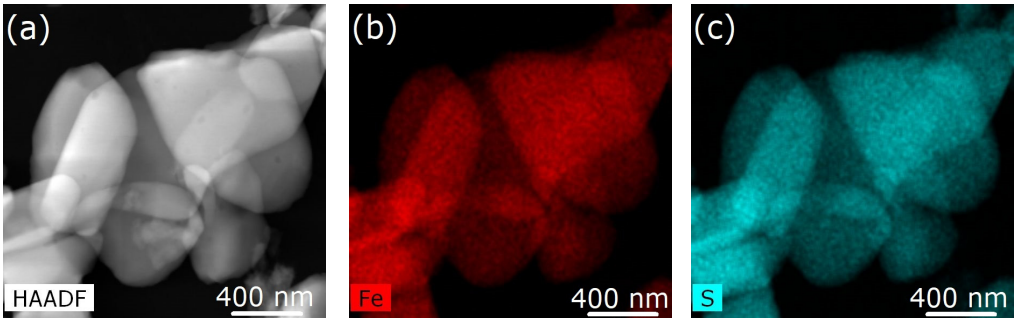

Figure 5. (**a**) Image of $Fe(phen)_2(NCS)_2$ plus PANI plus Fe_3O_4 nanoparticles (1% loading by weight) obtained using scanning transmission microscopy in high-angle annular dark-field mode. (**b**,**c**) Elemental mapping of iron and sulfur of the $[Fe(phen)_2(NCS)_2]$, respectively.

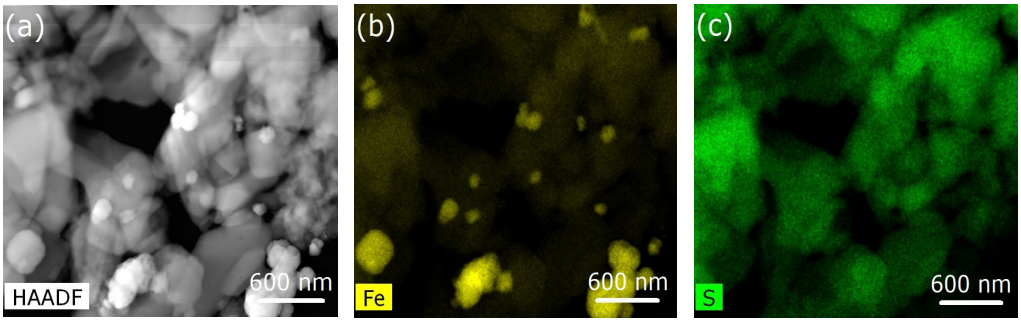

Figure 6. (**a**) Image of $Fe(phen)_2(NCS)_2$ plus PANI plus Fe_3O_4 nanoparticles (5% loading by weight) obtained using scanning transmission microscopy in high-angle annular dark-field mode. (**b**,**c**) Elemental mapping of iron and sulfur of the $[Fe(phen)_2(NCS)_2]$, respectively.

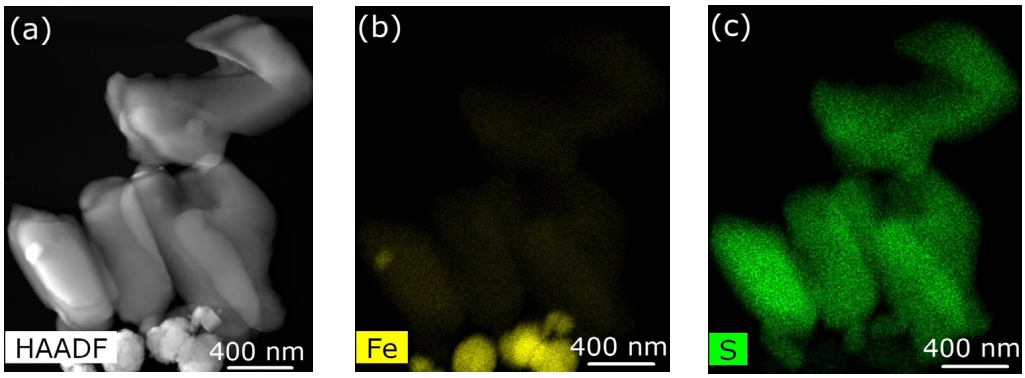

Figure 7. (**a**) Image of $Fe(phen)_2(NCS)_2$ plus PANI plus Fe_3O_4 nanoparticles (10% loading by weight) obtained using scanning transmission microscopy in high-angle annular dark-field mode. (**b**,**c**) Elemental mapping of iron and sulfur of the $[Fe(phen)_2(NCS)_2]$, respectively.

As shown in Figure 8, the addition of Fe_3O_4 nanoparticles to the $Fe(phen)_2(NCS)_2$ plus PANI composite leads to an increasing paramagnetic susceptibility background with an increasing concentration of Fe_3O_4 nanoparticles in the $Fe(phen)_2(NCS)_2$ plus PANI composite. In general, as shown in Figure 8, the paramagnetic susceptibility at a fixed temperature is linearly proportional to the concentration of Fe_3O_4 nanoparticles in the $Fe(phen)_2(NCS)_2$ plus PANI composite.

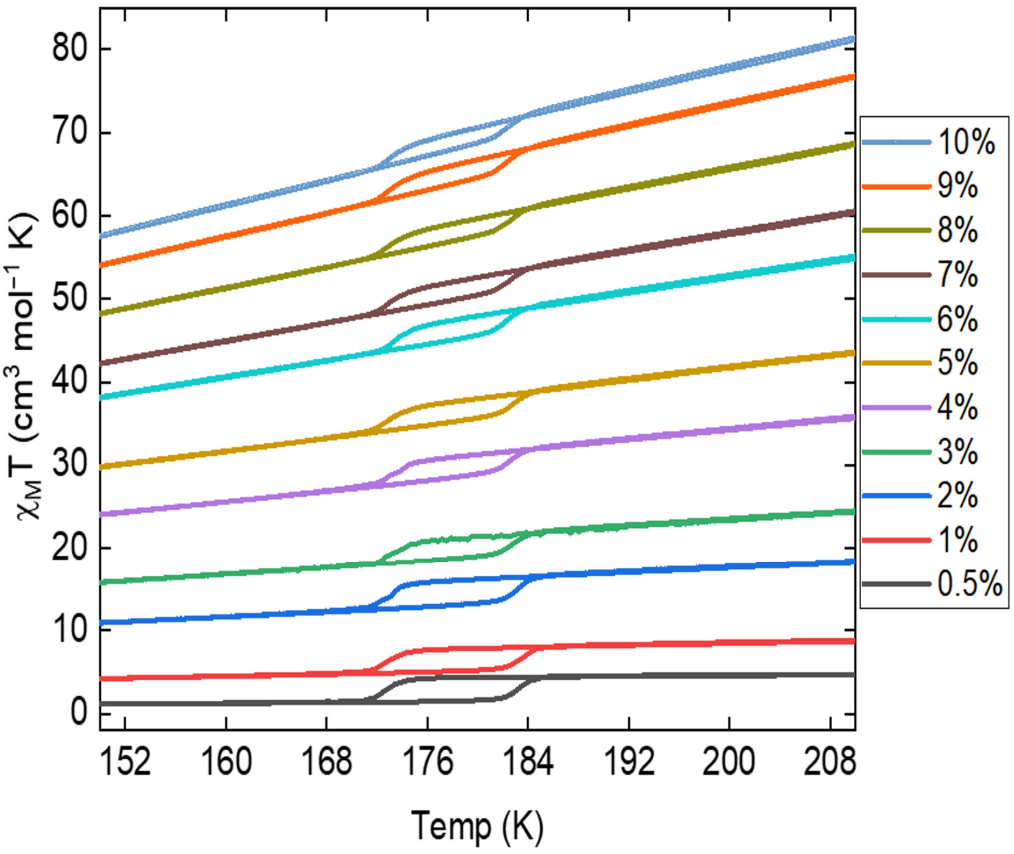

Figure 8. The $\chi_M T$ versus T plots for composites of $Fe(phen)_2(NCS)_2$ plus PANI plus varying concentrations of Fe_3O_4 (percent loading, by weight), with an applied magnetic field of 2 T.

The hysteresis width in the $\chi_m T$ versus T remains remarkably consistent, with changes no more than 2 K across varying concentrations of Fe_3O_4 nanoparticles in the $Fe(phen)_2(NCS)_2$ plus PANI composite (Figure 8, Supplementary Materials Table S1, Figures S2 and S3). These largely consistent hysteresis widths indicate that the cooperative effect seen for $Fe(phen)_2(NCS)_2$ is stable and remains unperturbed upon mixing with the PANI and the addition of Fe_3O_4 nanoparticles into the composite. This differs from the doped $Fe(phen)_2(NCS)_2$ thin film [38,39], where Mn doping has a profound effect on the hysteresis width in the temperature.

Above the spin state transition temperature, $Fe(phen)_2(NCS)_2$ has a significant magnetic moment that can overwhelm the moment from the Fe_3O_4 nanoparticles at very low Fe_3O_4 nanoparticle concentrations, as shown in the insets in Figures 9 and 10. For the $Fe(phen)_2(NCS)_2$ plus PANI plus Fe_3O_4 nanoparticle (1% loading by weight) composite, there is an increase in the XMCD signal at the Fe 2p core edges (Figure 10) as the $Fe(phen)_2(NCS)_2$ goes from the diamagnetic low spin state (at 80 K) to the paramagnetic high spin state (at 300 K). At higher Fe_3O_4 nanoparticle concentrations in the $Fe(phen)_2(NCS)_2$ plus PANI composite, the effect of the $Fe(phen)_2(NCS)_2$ spin state is more complex.

The XMCD response, Figure 10a, extracted from the XAS spectra (the insets in Figure 9 and Supplementary Materials Figures S5–S8) with oppositely applied magnetic fields does increase with increasing Fe_3O_4 nanoparticle concentrations when $Fe(phen)_2(NCS)_2$ is in the diamagnetic low spin state (at 80 K). The increase in the XMCD signal is not linear with respect to the increasing Fe_3O_4 nanoparticle concentration (Figure 11a). This is true even for Fe_3O_4 nanoparticles in the $Fe(phen)_2(NCS)_2$ plus PANI composite at 80 K, where $Fe(phen)_2(NCS)_2$ is in a low spin state (diamagnetic) and does not contribute to the net magnetization. The surmise is that the Fe_3O_4 nanoparticles are the primary overall

XMCD signal source when $Fe(phen)_2(NCS)_2$ is in a low spin state. This hypothesis that the Fe_3O_4 nanoparticles are the primary overall XMCD signal source when $Fe(phen)_2(NCS)_2$ is in a low spin state is consistent with the fact that below the spin crossover transition temperature (<172 K), the magnetic susceptibility is fairly constant in temperature. The non-linear increase in the XMCD signal with respect to the increasing concentrations of Fe_3O_4 nanoparticles can be attributed to the fact that the agglomeration of Fe_3O_4 nanoparticles (Figures 4b, 5b and 6b) is ferromagnetically coupled with the $Fe(phen)_2(NCS)_2$ in the $Fe(phen)_2(NCS)_2$ plus PANI composite, as the Fe_3O_4 nanoparticles aggregate.

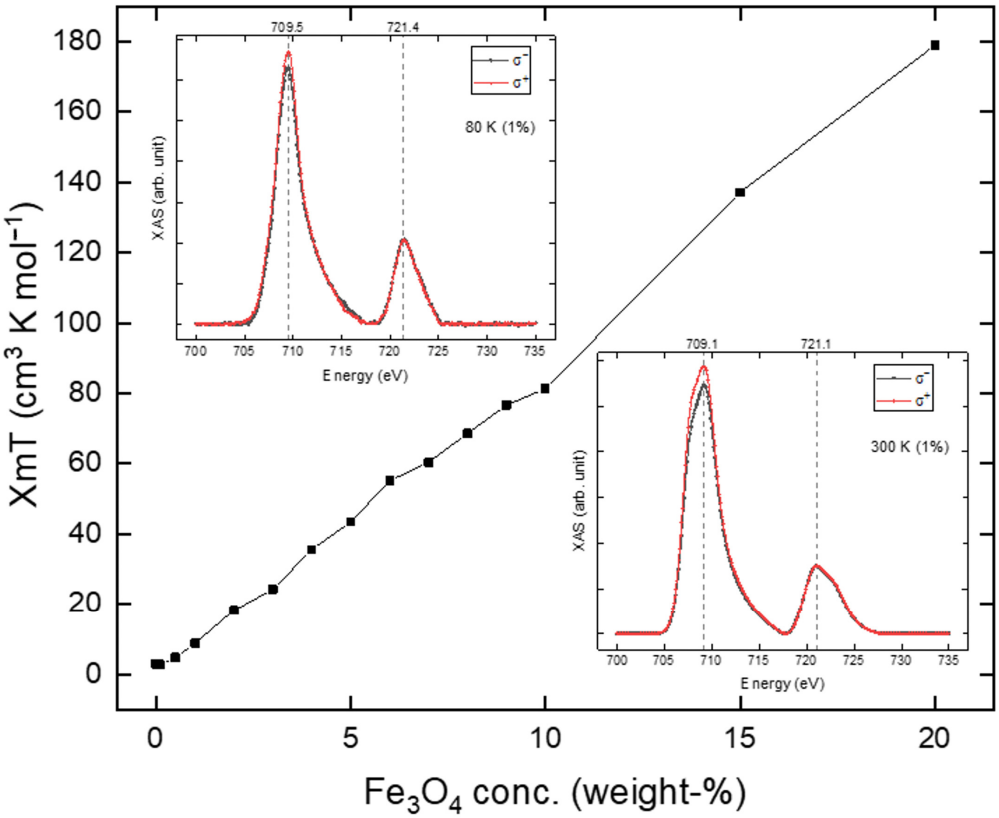

Figure 9. The value $\chi_M T$ is plotted as a function of the Fe_3O_4 nanoparticle concentration in $Fe(phen)_2(NCS)_2$ plus PANI composite, for T = 210 K. Insets are the X-ray absorption spectra of Fe L_3 ($2p_{3/2}$) and L_2 ($2p_{1/2}$) edges at 80 K (top left corner) and 300 K (bottom right corner) of the $Fe(phen)_2(NCS)_2$ plus PANI plus Fe_3O_4 (1% loading by weight).

Despite the fact that the magnetic susceptibility times temperature, $\chi_M T$, at a constant temperature of 210 K increases linearly with respect to an increasing concentration of the Fe_3O_4 nanoparticles, as shown in Figure 9, a comparison of the XMCD signal at the Fe L_3 ($2p_{3/2}$) edge in Figure 10b provides evidence that there is anti-ferromagnetic coupling between the Fe_3O_4 nanoparticles and the $Fe(phen)_2(NCS)_2$ in the $Fe(phen)_2(NCS)_2$ plus PANI plus Fe_3O_4 nanoparticles composite. Hence, there is an overall reduction in the XMCD signal (Figure 10b, Supplementary Figure S8), with an increasing concentration of Fe_3O_4 nanoparticles in the $Fe(phen)_2(NCS)_2$ plus PANI composite when the $[Fe(phen)_2(NCS)_2]$ is in a high spin state. The decrease in the XMCD response is rather significant, and, therefore, the antiferromagnetic coupling between both the $Fe(phen)_2(NCS)_2$ and the Fe_3O_4 nanoparticles cannot be restricted to only the $Fe(phen)_2(NCS)_2$ at the surface of the Fe_3O_4 nanoparticles. Furthermore, it implies that $Fe(phen)_2(NCS)_2$ retains nontrivial paramagnetic correlation lengths in PANI.

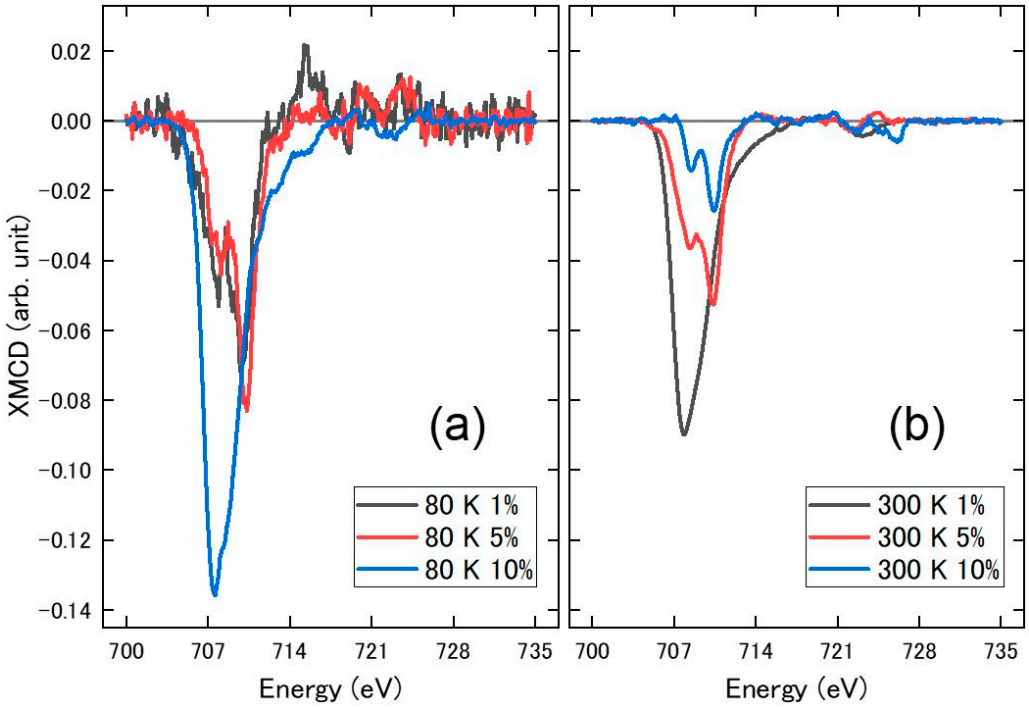

Figure 10. The Fe (L_3 and L_2 edges) XMCD signals for $Fe(phen)_2(NCS)_2$ plus PANI plus Fe_3O_4 nanoparticles (1%, 5% and 10% loading by weight). Data were taken for $Fe(phen)_2(NCS)_2$ in the low spin state (**a**) at 80 K and $Fe(phen)_2(NCS)_2$ in the high spin state (**b**) at 300 K.

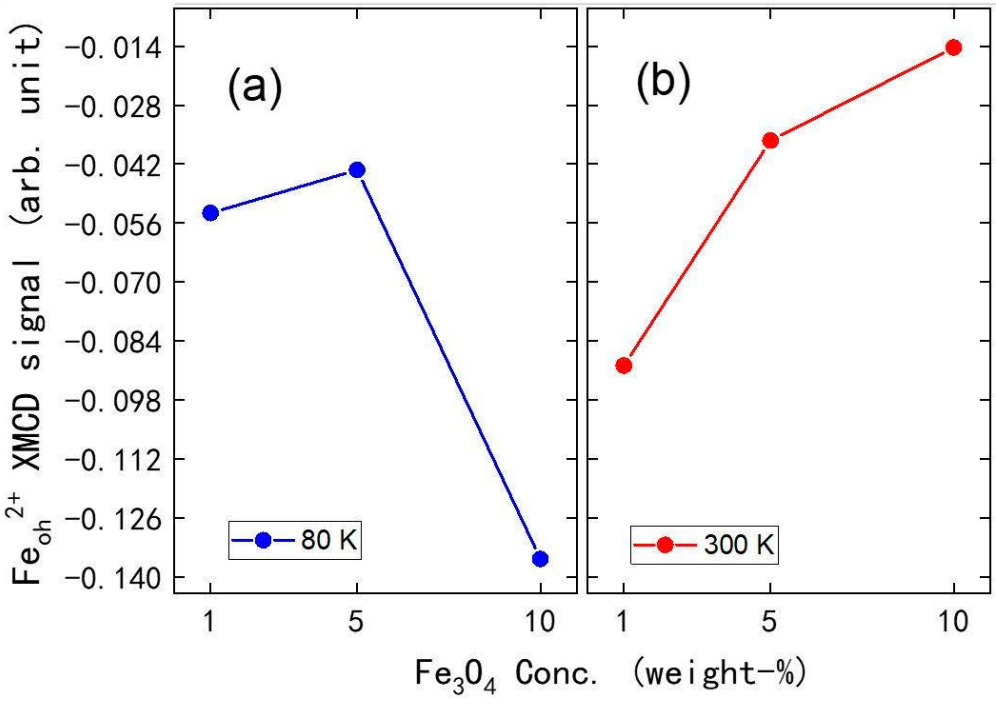

Figure 11. The XMCD signal of the Fe^{2+}_{Oh} site for varying concentrations (% by weight) of Fe_3O_4 nanoparticles in the $Fe(phen)_2(NCS)_2$ plus PANI composite at (**a**) 80 K and (**b**) 300 K.

5. I(V) Characteristics

The transport measurements also suggest that the behavior of $Fe(phen)_2(NCS)_2$ in the composites of $Fe(phen)_2(NCS)_2$ plus PANI plus Fe_3O_4 is not perturbed by the addition of Fe_3O_4 nanoparticles. The room temperature DC current-voltage I(V) measurement shown in Figure 12 is, in fact, characteristic of the transport behavior of $Fe(phen)_2(NCS)_2$ by

itself [21], which was carried out on thin films of $Fe(phen)_2(NCS)_2$ plus PANI plus Fe_3O_4 (10% loading by weight) drop-casted between two copper electrodes on a glass substrate without light illumination. As anticipated from the transport behavior of $Fe(phen)_2(NCS)_2$ by itself [21], the transport characteristic is Ohmic with a linear slope of 1.02, as plotted in the double log I(V) curve, Figure 12b, approximately below 0.6 V. Above 0.6 V, the transport characteristic remains linear with a slope of 1.38, which is an indication that it tends towards a space charge-limited current regime. Such space charge-limited current behavior of the $Fe(phen)_2(NCS)_2$ thin film itself has been reported previously with a linear slope of 2.04 [21]. The slope of 1.38 obtained in this study can be understood as a diminishing of the space charge with $Fe(phen)_2(NCS)_2$ in the PANI matrix. This further confirms that mixing $Fe(phen)_2(NCS)_2$ with the PANI, which is nominally a conducting polymer, reduces the overall on-state resistance.

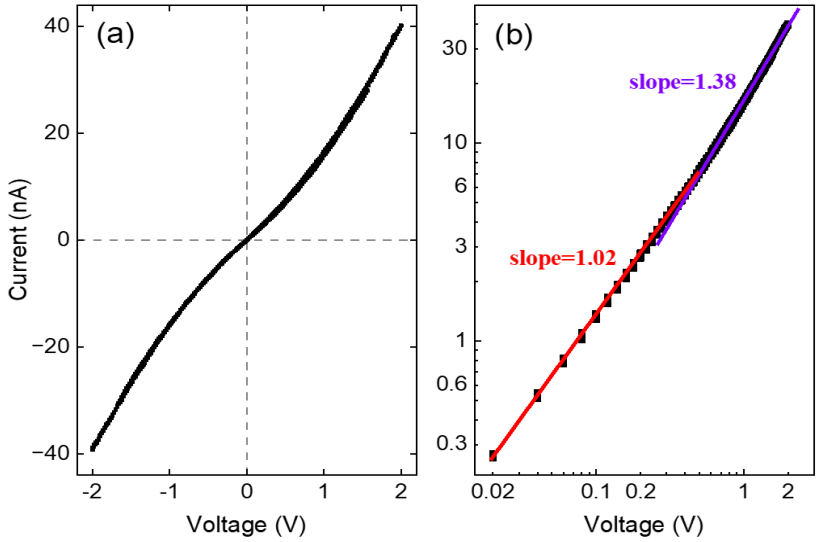

Figure 12. (**a**) The dc I(V) characteristics of $Fe(phen)_2(NCS)_2$ plus PANI plus Fe_3O_4 (10% by weight) and (**b**) double-log plot of the I(V) characteristics.

We can understand part of this overall behavior, i.e., the diminishing of the space charge, when different concentrations of Fe_3O_4 nanoparticles are added to the $Fe(phen)_2(NCS)_2$ plus PANI composite by noting that $Fe(phen)_2(NCS)_2$ remains uniformly mixed with PANI, at least on the scale of the scanning TEM, but as the concentration of Fe_3O_4 nanoparticles increases, the Fe_3O_4 nanoparticles are phase separated, as seen in Figures 4–6.

6. Summary

The cooperative effect, in general, is sensitive to the sample synthesis method [9,29,31,34,42]. Here, the hysteretic behavior of $Fe(phen)_2(NCS)_2$ is larger than generally observed. Yet the large hysteretic behavior of approximately 10 to 11 K is largely retained upon the addition of PANI and Fe_3O_4 nanoparticles, unlike what was observed with $[Fe(Htrz)_2(trz)](BF)_4$ combined with PANI [5] and Mn-doped $Fe(phen)_2(NCS)_2$ [38,39]. At the same time, the cooperative effect in this study is among the largest of those reported in the literature [27–34], although it is smaller than the 14 K inferred from [38]. While small groupings of $Fe(phen)_2(NCS)_2$ moieties may occur in the PANI matrix, there is no phase separation of the $Fe(phen)_2(NCS)_2$ from the PANI. In other words, the $Fe(phen)_2(NCS)_2$ tends to mix fairly homogeneously with the PANI.

The agglomeration of Fe_3O_4 nanoparticles, which is an indication of the phase separation of Fe_3O_4 nanoparticles in the $Fe(phen)_2(NCS)_2$ plus PANI composite, is observed and it is observed to be directly proportional to the concentration of Fe_3O_4 nanoparticles. However, the $Fe(phen)_2(NCS)_2$ spin crossover molecules remain uniformly distributed

within the PANI in all cases, which suggests that there exists a relatively high degree of miscibility.

Surprisingly, adding varying concentrations of Fe_3O_4 nanoparticles into the $Fe(phen)_2(NCS)_2$ plus PANI composite did not perturb the cooperativity. The hysteresis width in the $\chi_m T$ versus T for $Fe(phen)_2(NCS)_2$, at the spin state transition, remains consistent, with a hysteresis width change of less than 2 K throughout various concentrations of Fe_3O_4 nanoparticles in the $Fe(phen)_2(NCS)_2$ plus PANI composite. In addition, from the XMCD at the Fe edges, we observed that the overall XMCD signal does not increase in a linear fashion with respect to an increasing concentration of Fe_3O_4 nanoparticles in the $Fe(phen)_2(NCS)_2$ plus PANI composite. In addition, the phase-separated Fe_3O_4 nanoparticles in the $Fe(phen)_2(NCS)_2$ plus PANI composite tend to exhibit antiferromagnetic coupling between the nanoparticles and $Fe(phen)_2(NCS)_2$ when the latter is in the high spin state. The quenching of the XMCD signal with as much as 10% (loading by weight) of the Fe_3O_4 nanoparticles in the $Fe(phen)_2(NCS)_2$ plus PANI composite suggests that a considerable volume of $Fe(phen)_2(NCS)_2$ in the PANI is antiferromagnetically coupled to the Fe_3O_4.

Supplementary Materials: The following supporting information can be downloaded at https://www.mdpi.com/article/10.3390/molecules29194574/s1, Figure S1: The Fourier transform IR (FTIR) spectrum of $Fe(phen)_2(NCS)_2$ nano-powder that was used for all bi-composite and tri-composite fabrication; Table S1: The hysteresis width in $\chi_M T$ versus T plot for composites of $Fe(phen)_2(NCS)_2$ plus PANI plus varying concentrations of Fe_3O_4 (from 0.5 % up to 20 % by weight). The applied magnetic field is 2 T. Third column δ, is evaluated as the hysteresis width changes of that sample with respect to the hysteresis width of pristine $Fe(phen)_2(NCS)_2$, as the reference; Figure S2: The plots of $\chi_M T$ versus T for composites of $Fe(phen)_2(NCS)_2$ plus PANI plus various concentrations of Fe_3O_4 nanoparticles (% loading by weight) with an external applied magnetic field of 2 T; Figure S3: Plots of $\chi_M T$ versus T, for composites of $Fe(phen)_2(NCS)_2$ plus PANI plus varying concentrations of Fe_3O_4 (% by weight). The $\chi_M T$ versus T of (a) pristine $Fe(phen)_2(NCS)_2$ crystallites while $Fe(phen)_2(NCS)_2$ plus PANI is plotted in black, (b) $Fe(phen)_2(NCS)_2$ plus PANI plus 5% (by weight) of Fe_3O_4, (c) $[Fe(phen)_2(NCS)_2]$ plus PANI plus 1% (by weight) of Fe_3O_4, (d) $[Fe(phen)_2(NCS)_2]$ plus PANI plus 10% (by weight) of Fe_3O_4. The applied magnetic field is 2 T; Figure S4: The $\chi_M T$ versus T plot for (gray) $Fe(phen)_2(NCS)_2$ and (red) $Fe(phen)_2(NCS)_2$ plus PANI composite. The applied magnetic field is 2 T; Figure S5: The XAS spectra of $Fe(phen)_2(NCS)_2$ plus PANI plus and Fe_3O_4 nanoparticles (5% loading by weight) composite at 80 K; Figure S6: The XAS spectra of $Fe(phen)_2(NCS)_2$ plus PANI plus and Fe_3O_4 nanoparticles (10% loading by weight) composite at 80 K; Figure S7: The XAS spectra of $Fe(phen)_2(NCS)_2$ plus PANI plus and Fe_3O_4 nanoparticles (5% loading by weight) composite at 300 K; Figure S8: The XAS spectra of $Fe(phen)_2(NCS)_2$ plus PANI plus and Fe_3O_4 nanoparticles (10% loading by weight) composite at 300 K.

Author Contributions: Sample Preparation: B.T. and W.K.C.; Data Acquisition: W.K.C., B.T., M.Z.Z., A.S., G.V. and A.T.N.; Data Analysis: B.T., R.Y.L., P.A.D. and W.K.C.; Data Curation: W.K.C., R.Y.L., A.T.N. and P.A.D.; Manuscript Preparation: W.K.C. and P.A.D.; Final Manuscript Preparation: W.K.C., R.Y.L. and P.A.D.; Project Supervision: A.T.N., R.Y.L. and P.A.D.; Funding: R.Y.L. and P.A.D. All authors have read and agreed to the published version of the manuscript.

Funding: This work was supported by the National Science Foundation (NSF) through the NSF-DMR-EPM 2317464 (WKC, MZZ, GV, and PAD), EPSCoR RII Track-1: Emergent Quantum Materials and Technologies (EQUATE), award number OIA-2044049 (AS, RL) and NSF-PREM award number 1827690 (AS, RL and BT). LBNL was supported by the Office of Science, the Office of Basic Energy Sciences of the US DOE (Contract No. DE-AC02-05CH11231).

Data Availability Statement: The Data will gladly be made available upon request.

Acknowledgments: The research was performed in part at the Nebraska Nanoscale Facility: National Nanotechnology Coordinated Infrastructure which supported by the National Science Foundation under Award No. ECCS: 1542182.

Conflicts of Interest: The authors declare that they have no known competing financial or personal relationships with other people or organizations that could inappropriately influence (bias) their work.

References

1. Nieto-Castro, D.; Garcés-Pineda, F.A.; Moneo-Corcuera, A.; Sánchez-Molina, I.; Galán-Mascarós, J.R. Mechanochemical Processing of Highly Conducting Organic/Inorganic Composites Exhibiting Spin Crossover–Induced Memory Effect in Their Transport Properties. *Adv. Funct. Mater.* **2021**, *31*, 2102469. [CrossRef]
2. Joseph, A. *Modifying Magnetic Properties by Ion Irradiation or Light-Matter Coupling: Towards Innovative Magnetic Memory Devices*; L'université de Strasbourg: Strasbourg, France, 2024.
3. Mishra, E.; Ekanayaka, T.K.; McElveen, K.A.; Lai, R.Y.; Dowben, P.A. Evidence for long drift carrier lifetimes in $[Fe(Htrz)_2(trz)](BF_4)$ plus polyaniline composites. *Org. Electron.* **2022**, *105*, 106516. [CrossRef]
4. Dowben, P.A.; Mishra, E.; Ekanayaka, T.K.; Cheng, R. Progress towards the competitive multiferroic molecular transistor. In Proceedings of the 2023 IEEE Nanotechnology Materials and Devices Conference (NMDC), Paestum, Italy, 22–25 October 2023; pp. 626–627.
5. Mishra, E.; Chin, W.; McElveen, K.A.; Ekanayaka, T.K.; Zaz, M.Z.; Viswan, G.; Zielinski, R.; N'Diaye, A.T.; Shapiro, D.; Lai, R.Y.; et al. Electronic transport properties of spin-crossover polymer plus polyaniline composites with Fe_3O_4 nanoparticles. *J. Phys. Mater.* **2024**, *7*, 015010. [CrossRef]
6. Koo, Y.; Galán-Mascarós, J.R. Spin Crossover Probes Confer Multistability to Organic Conducting Polymers. *Adv. Mater.* **2014**, *26*, 6785–6789. [CrossRef]
7. Enriquez-Cabrera, A.; Rapakousiou, A.; Piedrahita Bello, M.; Molnár, G.; Salmon, L.; Bousseksou, A. Spin crossover polymer composites, polymers and related soft materials. *Coord. Chem. Rev.* **2020**, *419*, 213396. [CrossRef]
8. Kilic, M.S.; Brehme, J.; Pawlak, J.; Tran, K.; Bauer, F.W.; Shiga, T.; Suzuki, T.; Nihei, M.; Sindelar, R.F.; Renz, F. Incorporation and Deposition of Spin Crossover Materials into and onto Electrospun Nanofibers. *Polymers* **2023**, *15*, 2365. [CrossRef]
9. Tanasa, R.; Laisney, J.; Stancu, A.; Boillot, M.-L.; Enachescu, C. Hysteretic behavior of $Fe(phen)_2(NCS)_2$ spin-transition microparticles vs. the environment: A huge reversible component resolved by first order reversal curves. *Appl. Phys. Lett.* **2014**, *104*, 031909. [CrossRef]
10. Kahn, O.; Kröber, J.; Jay, C. Spin Transition Molecular Materials for displays and data recording. *Adv. Mater.* **1992**, *4*, 718–728. [CrossRef]
11. Kahn, O.; Martinez, C.J. Spin-Transition Polymers: From Molecular Materials Toward Memory Devices. *Science* **1998**, *279*, 44–48. [CrossRef]
12. Bousseksou, A.; Molnár, G.; Demont, P.; Menegotto, J. Observation of a thermal hysteresis loop in the dielectric constant of spin crossover complexes: Towards molecular memory devices. *J. Mater. Chem.* **2003**, *13*, 2069–2071. [CrossRef]
13. Bousseksou, A.; Molnár, G. The spin-crossover phenomenon: Towards molecular memories. *Comptes Rendus Chim.* **2003**, *6*, 1175–1183. [CrossRef]
14. Miyamachi, T.; Gruber, M.; Davesne, V.; Bowen, M.; Boukari, S.; Joly, L.; Scheurer, F.; Rogez, G.; Yamada, T.K.; Ohresser, P.; et al. Robust spin crossover and memristance across a single molecule. *Nat. Commun.* **2012**, *3*, 938. [CrossRef]
15. Kuch, W.; Bernien, M. Controlling the magnetism of adsorbed metal–organic molecules. *J. Phys. Condens. Matter* **2017**, *29*, 023001. [CrossRef]
16. Prins, F.; Monrabal-Capilla, M.; Osorio, E.A.; Coronado, E.; van der Zant, H.S.J. Room-Temperature Electrical Addressing of a Bistable Spin-Crossover Molecular System. *Adv. Mater.* **2011**, *23*, 1545–1549. [CrossRef]
17. Ekanayaka, T.K.; Hao, G.; Mosey, A.; Dale, A.S.; Jiang, X.; Yost, A.J.; Sapkota, K.R.; Wang, G.T.; Zhang, J.; N'Diaye, A.T.; et al. Nonvolatile Voltage Controlled Molecular Spin-State Switching for Memory Applications. *Magnetochemistry* **2021**, *7*, 37. [CrossRef]
18. Zaz, M.Z.; Ekanayaka, T.K.; Cheng, R.; Dowben, P.A. Variability of the Conductance Changes Associated with the Change in the Spin State in Molecular Spin Crossover Complexes. *Magnetochemistry* **2023**, *9*, 223. [CrossRef]
19. Zhang, Y.; Zhang, L.; Ridier, K.; Salmon, L.; Séguy, I.; Molnár, G.; Bousseksou, A. Switching endurance of the molecular spin crossover complex $[Fe(HB(tz)_3)_2]$: From single crystals to thin films and electronic devices. *Mater. Adv.* **2022**, *3*, 8193–8200. [CrossRef]
20. Zhang, Y.; Séguy, I.; Ridier, K.; Shalabaeva, V.; Piedrahita-Bello, M.; Rotaru, A.; Salmon, L.; Molnár, G.; Bousseksou, A. Resistance switching in large-area vertical junctions of the molecular spin crossover complex $[Fe(HB(tz)_3)_2]$: ON/OFF ratios and device stability. *J. Phys. Condens. Matter* **2020**, *32*, 214010. [CrossRef]
21. Shi, S.; Schmerber, G.; Arabski, J.; Beaufrand, J.-B.; Kim, D.J.; Boukari, S.; Bowen, M.; Kemp, N.T.; Viart, N.; Rogez, G.; et al. Study of molecular spin-crossover complex $Fe(phen)_2(NCS)_2$ thin films. *Appl. Phys. Lett.* **2009**, *95*, 043303. [CrossRef]
22. Real, J.A.; Gallois, B.; Granier, T.; Suez-Panama, F.; Zarembowitch, J. Comparative investigation of the spin-crossover compounds $Fe(btz)_2(NCS)_2$ and $Fe(phen)_2(NCS)_2$ (where btz = 2,2′-bi-4,5-dihydrothiazine and phen = 1,10-phenanthroline). Magnetic properties and thermal dilatation behavior and crystal structure of $Fe(btz)_2(NCS)_2$ at 293 and 130 K. *Inorg. Chem.* **1992**, *31*, 4972–4979. [CrossRef]
23. Ellingsworth, E.C.; Turner, B.; Szulczewski, G. Thermal conversion of $[Fe(phen)_3](SCN)_2$ thin films into the spin crossover complex $Fe(phen)_2(NCS)_2$. *RSC Adv.* **2013**, *3*, 3745. [CrossRef]
24. Laisney, J.; Tissot, A.; Molnár, G.; Rechignat, L.; Rivière, E.; Brisset, F.; Bousseksou, A.; Boillot, M.-L. Nanocrystals of $Fe(phen)_2(NCS)_2$ and the size-dependent spin-crossover characteristics. *Dalt. Trans.* **2015**, *44*, 17302–17311. [CrossRef] [PubMed]
25. Enachescu, C.; Tanasa, R.; Stancu, A.; Tissot, A.; Laisney, J.; Boillot, M.-L. Matrix-assisted relaxation in $Fe(phen)_2(NCS)_2$ spin-crossover microparticles, experimental and theoretical investigations. *Appl. Phys. Lett.* **2016**, *109*, 031908. [CrossRef]

26. Beniwal, S.; Sarkar, S.; Baier, F.; Weber, B.; Dowben, P.A.; Enders, A. Site selective adsorption of the spin crossover complex $Fe(phen)_2(NCS)_2$ on Au(111). *J. Phys. Condens. Matter* **2020**, *32*, 324003. [CrossRef]
27. Bousseksou, A.; Negre, N.; Goiran, M.; Salmon, L.; Tuchagues, J.P.; Boillot, M.L.; Boukheddaden, K.; Varret, F. Dynamic triggering of a spin-transition by a pulsed magnetic field. *Eur. Phys. J. B* **2000**, *13*, 451–456. [CrossRef]
28. Zhang, X.; Mu, S.; Chastanet, G.; Daro, N.; Palamarciuc, T.; Rosa, P.; Létard, J.-F.; Liu, J.; Sterbinsky, G.E.; Arena, D.A.; et al. Complexities in the Molecular Spin Crossover Transition. *J. Phys. Chem. C* **2015**, *119*, 16293–16302. [CrossRef]
29. Sorai, M.; Seki, S. Phonon coupled cooperative low-spin $^1A_1$high-spin $^5T_2$ transition in $[Fe(phen)_2(NCS)_2]$ and $[Fe(phen)_2(NCSe)_2]$ crystals. *J. Phys. Chem. Solids* **1974**, *35*, 555–570. [CrossRef]
30. Gallois, B.; Real, J.A.; Hauw, C.; Zarembowitch, J. Structural changes associated with the spin transition in bis(isothiocyanato) bis(1,10-phenanthroline)iron: A single-crystal x-ray investigation. *Inorg. Chem.* **1990**, *29*, 1152–1158. [CrossRef]
31. Valverde-Muñoz, F.J.; Gaspar, A.B.; Shylin, S.I.; Ksenofontov, V.; Real, J.A. Synthesis of Nanocrystals and Particle Size Effects Studies on the Thermally Induced Spin Transition of the Model Spin Crossover Compound $[Fe(phen)_2(NCS)_2]$. *Inorg. Chem.* **2015**, *54*, 7906–7914. [CrossRef]
32. Granier, T.; Gallois, B.; Gaultier, J.; Real, J.A.; Zarembowitch, J. High-pressure single-crystal x-ray diffraction study of two spin-crossover iron(II) complexes: $Fe(Phen)_2(NCS)_2$ and $Fe(Btz)_2(NCS)_2$. *Inorg. Chem.* **1993**, *32*, 5305–5312. [CrossRef]
33. Qi, Y.; Müller, E.W.; Spiering, H.; Gütlich, P. The effect of a magnetic field on the high-spin α low-spin transition in $[Fe(phen)_2(NCS)_2]$. *Chem. Phys. Lett.* **1983**, *101*, 503–505. [CrossRef]
34. Müller, E.W.; Spiering, H.; Gütlich, P. Spin transition in $[Fe(phen)_2(NCS)_2]$ and $[Fe(bipy)_2(NCS)_2]$: Hysteresis and effect of crystal quality. *Chem. Phys. Lett.* **1982**, *93*, 567–571. [CrossRef]
35. Bousseksou, A.; McGarvey, J.J.; Varret, F.; Real, J.A.; Tuchagues, J.-P.; Dennis, A.C.; Boillot, M.L. Raman spectroscopy of the high- and low-spin states of the spin crossover complex $Fe(phen)_2(NCS)_2$: An initial approach to estimation of vibrational contributions to the associated entropy change. *Chem. Phys. Lett.* **2000**, *318*, 409–416. [CrossRef]
36. Bertoni, R.; Lorenc, M.; Graber, T.; Henning, R.; Moffat, K.; Létard, J.-F.; Collet, E. Cooperative elastic switching vs. laser heating in $[Fe(phen)_2(NCS)_2]$ spin-crossover crystals excited by a laser pulse. *CrystEngComm* **2016**, *18*, 7269–7275. [CrossRef]
37. Gruber, M.; Miyamachi, T.; Davesne, V.; Bowen, M.; Boukari, S.; Wulfhekel, W.; Alouani, M.; Beaurepaire, E. Spin crossover in $Fe(phen)_2(NCS)_2$ complexes on metallic surfaces. *J. Chem. Phys.* **2017**, *146*, 092312. [CrossRef]
38. Saha, S.; Chandra, P.; Mandal, S.K. Spin state bistability in (Mn, Zn) doped $Fe(phen)_2(NCS)_2$ molecular thin film nanocrystals on quartz. *Physica B* **2022**, *642*, 414128. [CrossRef]
39. Saha, S.; Mandal, S.K. Spin transition properties of metal (Zn, Mn) diluted $Fe(phen)_2(NCS)_2$ spin-crossover thin films. *Eur. Phys. J. Appl. Phys.* **2020**, *91*, 20301. [CrossRef]
40. Saha, S.; Mandal, S.K. Methanol sensing characteristics in undoped and (Zn, Mn) doped $Fe(phen)_2(NCS)_2$ spin-crossover thin films. *Mater. Today Proc.* **2022**, *66*, 3387–3391. [CrossRef]
41. Tissot, A.; Enachescu, C.; Boillot, M.L. Control of the thermal hysteresis of the prototypal spin-transition $Fe^{II}(phen)_2(NCS)_2$ compound via the microcrystallites environment: Experiments and mechanoelastic model. *J. Mater. Chem.* **2012**, *22*, 20451–20457. [CrossRef]
42. Akabori, K.; Matsuo, H.; Yamamoto, Y. Thermal properties of tris(1,10-phenanthroline) complexes of iron(II) and nickel(II) salts. *J. Inorg. Nucl. Chem.* **1973**, *35*, 2679–2690. [CrossRef]
43. Tang, S.-J.; Wang, A.-T.; Lin, S.-Y.; Huang, K.-Y.; Yang, C.-C.; Yeh, J.-M.; Chiu, K.-C. Polymerization of aniline under various concentrations of APS and HCl. *Polym. J.* **2011**, *43*, 667–675. [CrossRef]
44. Adams, P.N.; Laughlin, P.J.; Monkman, A.P.; Kenwright, A.M. Low temperature synthesis of high molecular weight polyaniline. *Polymer* **1996**, *37*, 3411–3417. [CrossRef]
45. Ekanayaka, T.K.; Maity, K.P.; Doudin, B.; Dowben, P.A. Dynamics of Spin Crossover Molecular Complexes. *Nanomaterials* **2022**, *12*, 1742. [CrossRef] [PubMed]
46. Hao, G.; Dale, A.S.; N'Diaye, A.T.; Chopdekar, R.V.; Koch, R.J.; Jiang, X.; Mellinger, C.; Zhang, J.; Cheng, R.; Xu, X.; et al. Intermolecular interaction and cooperativity in an Fe(II) spin crossover molecular thin film system. *J. Phys. Condens. Matter* **2022**, *34*, 295201. [CrossRef]
47. Hauser, A.; Jeftić, J.; Romstedt, H.; Hinek, R.; Spiering, H. Cooperative phenomena and light-induced bistability in iron(II) spin-crossover compounds. *Coord. Chem. Rev.* **1999**, *190–192*, 471–491. [CrossRef]
48. Félix, G.; Nicolazzi, W.; Salmon, L.; Molnár, G.; Perrier, M.; Maurin, G.; Larionova, J.; Long, J.; Guari, Y.; Bousseksou, A. Enhanced Cooperative Interactions at the Nanoscale in Spin-Crossover Materials with a First-Order Phase Transition. *Phys. Rev. Lett.* **2013**, *110*, 235701. [CrossRef]